

# Spiral waves and the secondary in the novalike variable, V3885 Sgr

Louise E. Hartley<sup>1</sup>, James R. Murray<sup>1\*</sup>, Janet E. Drew<sup>2</sup>, Knox S. Long<sup>3</sup>

<sup>1</sup>*Mail number 31, Swinburne University of Technology, PO Box 218, Hawthorn, Victoria 3122, Australia*

<sup>2</sup>*Astrophysics Group, Imperial College London, Blackett Laboratory, Prince Consort Road, London, SW7 2AZ, UK*

<sup>3</sup>*Space Telescope Science Institute, 3700 San Martin Drive, Baltimore, MD 21218, USA*

5 February 2008

## ABSTRACT

We present seven nights' blue (4300–5000Å) spectroscopy of the novalike variable star, V3885 Sgr. The line spectrum shows a typical combination of broad absorption and emission in  $H\gamma$  and  $H\beta$  and He I, which is associated with the accretion disk. We also observe anti-phased narrow emission, which we attribute to irradiation of the secondary star. The He II  $\lambda 4686$  and N III–C III–C IV emission lines are devoid of structure and are most likely formed in an outflow. We measure radial velocity shifts in the absorption and emission lines, from which we fit an orbital period of  $4.97126 \pm 0.00036$  h. From the velocity semi-amplitudes of the disk and companion star, we are able to constrain the binary mass ratio to  $q > 0.7$ .

The phase-folded spectra provide dense coverage of the entire orbital cycle. Doppler tomograms of the hydrogen and He I lines reveal spiral structure in the accretion disk and the irradiated donor star. We believe this is the first unambiguous detection of spiral waves in a novalike variable.

**Key words:** accretion, accretion disks – binaries: close – binaries: spectroscopic – line: profiles – novae, cataclysmic variables – stars: individual (V3885 Sgr)

## 1 INTRODUCTION

V3885 Sgr is a bright ( $m_v = 10.4$ ) Cataclysmic Variable, an interacting binary system consisting of a white dwarf that accretes matter from a low-mass companion. V3885 Sgr belongs to the novalike subclass. The white dwarf accretes via a disk, yet the disk does not undergo outbursts in luminosity, as in dwarf novae. Rather, it persists in an outburst state with only small fluctuations in luminosity of a few tenths of a magnitude.

In understanding the processes of disk accretion, the novalike systems are valuable tools, because the accretion disk dominates the system luminosity and is thermally stable. Yet, it is precisely because the disk continually outshines the component stars that it is exceedingly difficult to measure the parameters of these binary systems with any accuracy.

There have been several attempts to determine the orbital period of V3885 Sgr. First Cowley, Crampton, & Hesser (1977) derived an orbital period  $P = 5.04$  h from radial velocity shifts in Balmer lines, seen mainly in absorption. Their observations seem to have been gathered during four spells of around 2.5 h each, spanning three days. Then Haug & Drechsel (1985)

used essentially the same spectroscopic technique and emerged with a very different period of 6.216 h. There were other peaks in the power spectrum they derived that were scarcely less pronounced, but none matched the period found by the earlier study. Haug & Drechsel gathered data on three occasions, spanning 2 months, adding to a total of  $\sim 12$  h observation. Finally Metz (1989) gave a period of 5.191 h, without ever presenting the experimental method clearly, yet this is the most commonly quoted period.

V3885 Sgr has been observed repeatedly in the ultraviolet by the *International Ultraviolet Explorer* (IUE) (Woods et al. 1992) and, more recently, by the *Hubble Space Telescope* (Hartley et al. 2002). The ultraviolet spectrum is dominated by strong wind-formed line profiles, but Hartley et al. found a surprising absence of short-timescale variability. Ultimately our interpretation of the ultraviolet spectrum was hampered by an inability to separate stochastic wind-formed features from phase-dependent variability. Therefore, we set out to firmly establish the orbital period of V3885 Sgr, by measuring radial velocity shifts in the blue ( $\sim 4200 - 5100\text{\AA}$ ) line spectrum.

The observations are detailed in Section 2. In Section 3 we present our measurement of the orbital period. Then in Section 4 we examine the line variability in more detail,

\* E-mail: jmurray@swin.edu.au

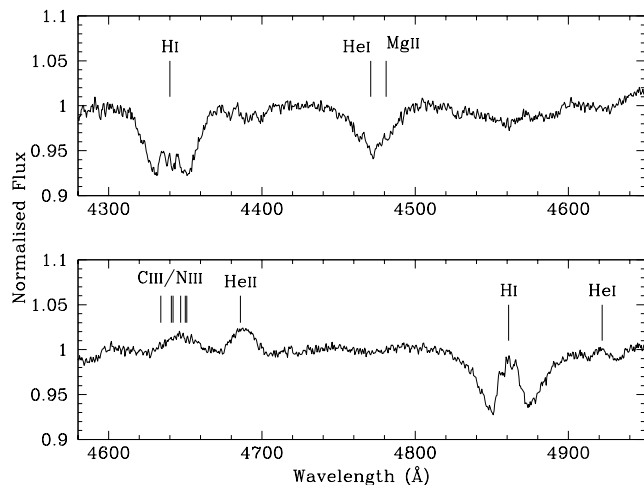


**Figure 1.** The time-averaged spectrum of V3885 Sgr, as observed at the SAAO in September 2003.

using Doppler tomography to reveal the secondary star and structure in the accretion disk.

## 2 THE OBSERVATIONS

We carried out seven nights of observations, during 2003 September 2–9, at the South African Astronomical Observatory’s (SAAO) 1.9-m telescope. The telescope was equipped with the grating spectrograph and SITe CCD. We used the number 4 grating, which gives a first-order central wavelength of 4600 Å and range of 800 Å. V3885 Sgr’s optical brightness enabled us to take advantage of the narrow, 200- $\mu$ m slit, which provides a spectral resolution of  $\sim 1$  Å. With an average exposure time of 300 s, this setup yields a  $S/N \sim 25$  per exposure.

To ensure good wavelength calibration, CuAr arc exposures were taken about every 15 min. Also, comparison observations of the radial velocity standard, HD187474, were made each night. In total, 300 useful spectra of V3885 Sgr were obtained over the seven nights and the good weather conditions allowed us to record some data every night.

Fig. 1 shows a normalised spectrum created from the sum of all the exposures. The spectrum shows the same line features as seen in Haug & Drechsel (1985), albeit at significantly higher  $S/N$ . The line spectrum is typical of a mid-inclination novalike variable: the line profiles are weak, consisting of broad Balmer and He I absorption, with superposed emission and weak emission in C III/N III and He II (see Section 4).

## 3 THE ORBITAL PERIOD

Measuring radial velocity variations in the absorption and emission lines made more difficult by the presence of several components that make up each line. The hydrogen lines consist of broad absorption, broad emission and narrow emission (see Section 4). As these components may be formed in distinct parts of the system, each had to be isolated and its

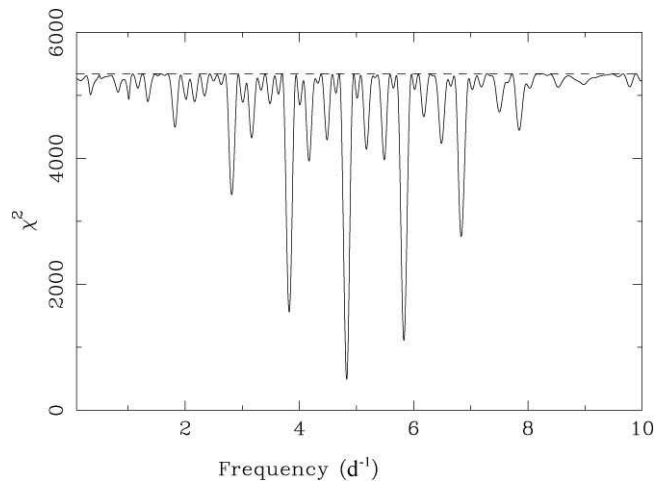


**Figure 2.** A sample  $\chi^2$ -frequency plot, for the  $H\beta$  line.

radial velocity measured independently of the other components.

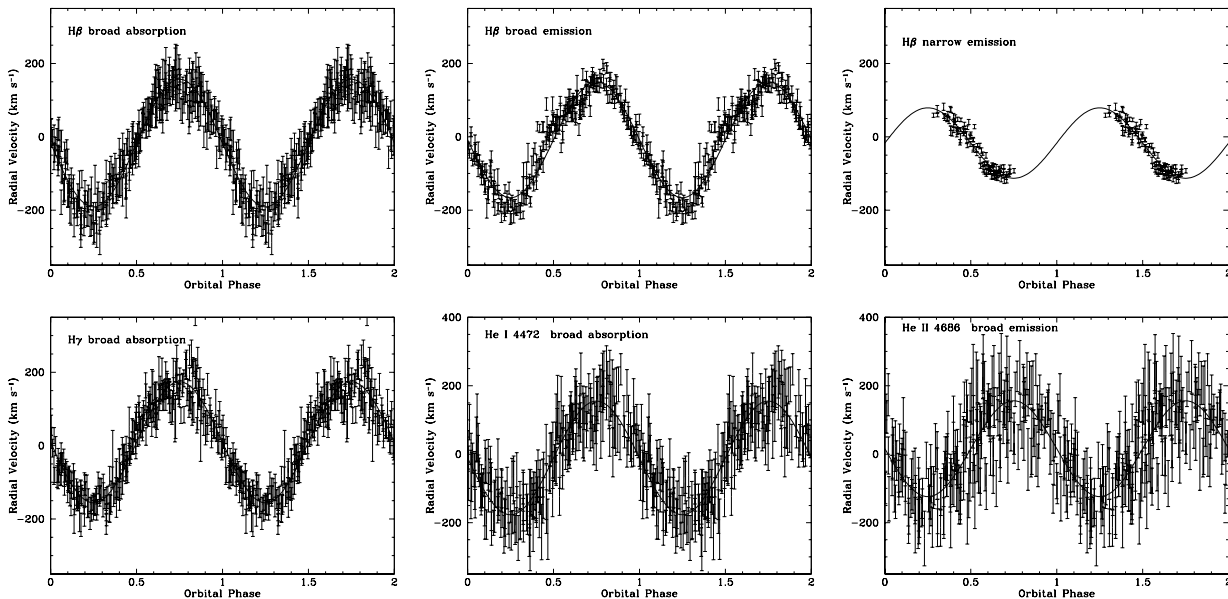
A least-squares method was used to fit Gaussians to each line component. For each line component the FWHM was held constant, depending on the line and the width of that feature. For the broad absorption the central portion of the line containing the emission components was masked out by eye and a Gaussian fitted to the line wings. For the broad emission the narrow emission (where present) and central double peak were masked out and two-component Gaussian was fit to the emission and the underlying broad absorption (to remove the latter). This fit was then subtracted from the line profile in order to measure the narrow emission component.

The best-fit radial velocity curve was found by folding the data on a range of trial frequencies and finding the lowest  $\chi^2$  sine curve at each frequency (software supplied by T. Marsh, private communication). A plot of  $\chi^2$  against frequency (see Fig. 2) shows the most likely frequency. As expected for nightly sampling, there are period aliases at  $\pm 1$  d from the strongest alias. However, the second strongest alias has a  $\chi^2$  of more than double that of the strongest alias and so we can be confident that the latter is the correct spectroscopic period.

The Gaussian fit technique worked well for the  $H\beta$  line. However, we found that the  $H\gamma$  broad absorption is not well fit by a Gaussian; it has steeper absorption wings, which descend abruptly from the continuum. To measure shifts in this line, we instead used a cross-correlation technique. First a template spectrum was created. The spectra were assigned radial velocities according to that measured for  $H\beta$  and then the corresponding radial velocities were subtracted from the wavelength scale of each spectrum. These spectra were summed to create a radial-velocity corrected template. After masking out all but the wings of the  $H\gamma$  line, each spectrum was cross-correlated with this template. This method was also used for the He I  $\lambda 4472$  absorption and He II  $\lambda 4686$  emission lines. Results of the radial-velocity measurements are listed in Table 1. Fig. 3 shows the radial velocity points, folded at their least- $\chi^2$  period for each of the  $H\beta$  line features.

The periods derived from the measured features agree

Line	$K$ ( $\text{km s}^{-1}$ )	$\gamma$ ( $\text{km s}^{-1}$ )	$P_{\text{orb}}$ (h)	$T_0$ (MHJD)	N. Points	$\chi^2_\nu$
H $\beta$ broad absorption and emission	163(2)	-10(2)	4.9724(10)	52887.85890(04)	575	3.68
H $\beta$ narrow emission	97(2)	-19(5)	4.9721(12)	52887.9659(20)	105	8.05
H $\gamma$ broad absorption	165(6)	<sup>a</sup>	4.9697(19)	52887.85911(08)	285	1.70
He I $\lambda$ 4472 broad absorption	166(10)	<sup>a</sup>	4.9682(38)	52887.8654(19)	225	1.15
He II $\lambda$ 4686 broad emission	135(10)	<sup>a</sup>	4.9730(55)	52887.8595(24)	224	2.03

<sup>a</sup>Measured from cross correlation of template spectrum, so no direct measurement of  $\gamma$ .**Table 1.** Parameters of radial-velocity fits to spectral lines in the blue spectrum of V3885 Sgr. Errors in parentheses are  $2\sigma$  limits.**Figure 3.** Radial velocity curves of shifts in the absorption and emission lines, folded on the orbital period. Top row, H $\beta$ : broad absorption, broad emission and narrow emission. Bottom row: H $\gamma$  broad absorption, He I  $\lambda$  4472 broad absorption and He II  $\lambda$  4686 broad emission.

to within the errors and a weighted mean gives an orbital period of  $4.97126 \pm 0.00036$  h. To within the errors the H $\beta$  narrow emission moves in exact anti-phase to the other lines. Setting aside the H $\beta$  narrow emission, we obtain an average zero-phase of  $52887.8602 \pm 0.0052$  MHJD, which refers to the epoch of red-to-blue crossing of the line features. If we assume that these features are formed in or above the accretion disk, this is inferior conjunction of the secondary star.

We find good agreement between the  $K$ -velocities obtained from the H $\beta$ , H $\gamma$  and He I  $\lambda$  4472 lines, with an average  $K = 166 \pm 6 \text{ km s}^{-1}$ . He II  $\lambda$  4686 is fit by a lower  $K$ -velocity of  $135 \pm 10 \text{ km s}^{-1}$ . A close inspection of a trailed spectrum reveals a very slight weakening of the short-wavelength edge of the He II line at around phase 0.25. This may account for the lower measured  $K$ -velocity. To improve the cross-correlation in this range of the spectrum, we attempted to measure He II  $\lambda$  4686 together with the 4630–4660 Å blend, however the latter was too weak in the individual spectra to give a reliable measurement.

#### 4 LINE PROFILES

We find the optical spectrum of V3885 Sgr unchanged since the 1982 observations of Haug & Drechsel (1985). The Balmer lines (H $\beta$  and H $\gamma$ ) show broad absorption, of a full width at the continuum  $\sim 5000 \text{ km s}^{-1}$ , and complex emission cores (see Section 4.1). He I  $\lambda$  4472 is also seen as broad absorption, with some structured emission near line centre. Other He I lines at 4387, 4713 and 4922 Å can be seen as weak absorption/emission lines.

The broad H I and He I absorption line profiles remain very constant in shape over the orbital period and their width suggests they are formed in the optically thick accretion disk.

Weak emission lines of  $\text{FWZI} \simeq 2000 \text{ km s}^{-1}$  are present in the carbon/nitrogen blend at 4650 Å and He II  $\lambda$  4686 line. This broad emission appears devoid of the emission structure associated with the broad absorption lines. The 4630–4660 Å blend is commonly thought to be comprised of C III and N III emission. However, a Gaussian fit that imposes the correct relative multiplet wavelengths of the N III, C III and C IV components indicates that the line profile is better emulated with a non-negligible C IV contribution.

The He II  $\lambda$  4686 emission profile probably forms mainly

in an outflow. It is no wider in velocity terms than the UV wind-dominated He II  $\lambda 1640$  absorption (see Hartley et al. 2002) and the lower level of the 4686 Å line is the upper level of He II  $\lambda 1640$ , so He II  $\lambda 4686$  can be recombination dominated even when He II  $\lambda 1640$  is in absorption. Furthermore any outflow may degrade the radiation field irradiating the outer disk, eliminating He<sup>+</sup> ionising photons. So we need not see any He II  $\lambda 4686$  structure associated with secondary or disc warps. Also, the He II  $\lambda 4686$  emission shifts velocity in phase with the disk-formed H  $\beta$  line (Table 1 and Figure 3), but by a slightly smaller amount ( $K=135 \text{ km s}^{-1}$ , compared to  $166 \text{ km s}^{-1}$ ). We suspect either blueshifted absorption and/or opacity effects cause us to detect only flux from the nearside of the white dwarf, thus distorting the velocity profile. The C III–N III–C IV line is too weak to measure its velocity shifts. However, its similarity to He II  $\lambda 4686$  indicate that this feature is also most likely to be formed in the same region.

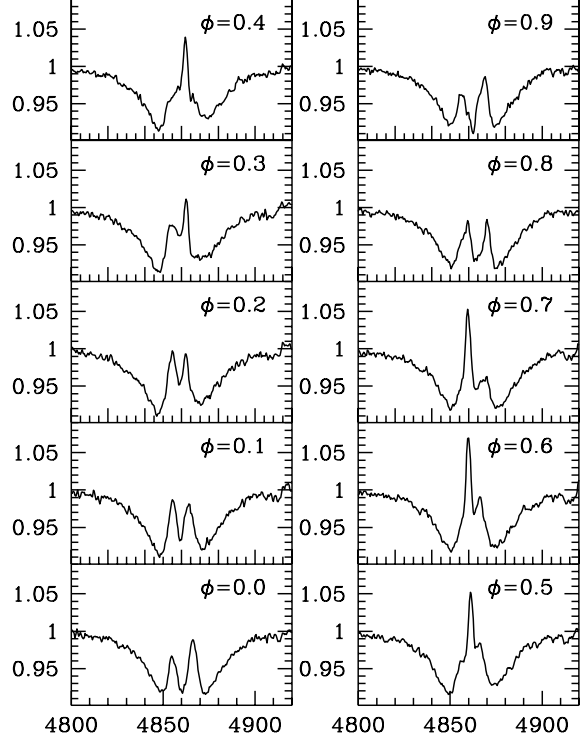
#### 4.1 Structure in the accretion disk

Fig. 4 shows the variation of the H  $\beta$  line profile over an orbital cycle. The H  $\gamma$  and He I  $\lambda 4472$  lines undergo similar changes in shape, although in those lines, the ratio of emission to absorption is smaller. The complex time-variable emission, which is superposed onto the broad absorption can be deconvolved into two components: broad emission of  $\text{FWHM} \simeq 700 \text{ km s}^{-1}$  and narrow emission of  $\text{FWHM} \simeq 150\text{--}200 \text{ km s}^{-1}$  (see Section 4.2). At those phases when the narrow emission is not seen ( $\phi \simeq 0.8\text{--}0.2$ ) the broad emission can in fact be seen to be double-peaked and composed of two emission profiles of  $\text{FWHM} \simeq 400 \text{ km s}^{-1}$ , with peaks separated by about  $600 \text{ km s}^{-1}$ .

The dense phase-coverage of our spectra lends them well to Doppler-mapping techniques (Marsh & Horne 1988). Trained spectra were made by normalising each spectrum by the time-average and then stacking the resultant spectra. These trained spectra were the input for the Doppler mapping. We succeeded in making Doppler maps from trained spectra of the H  $\gamma$ , H  $\beta$ , He I  $\lambda 4371$  and He I  $\lambda 4922$  lines. Attempts were made to create a Doppler map from He II  $\lambda 4686$ , but the map did not converge on any particular distribution of He II, probably because of the low S/N ratio of this line.

The maps were created using an entropy maximisation technique (T. Marsh, private communication). These are shown in Figs. 5 to 7. The maps require the systemic ( $\gamma$ ) velocity as an input parameter. We used the H  $\beta$   $\gamma$  velocity of  $-19 \text{ km s}^{-1}$ . The Roche lobe, centres of mass and accretion stream, which are overplotted on the maps are for arbitrary input parameters of  $M_1=0.7M_\odot$ ,  $M_2=0.6M_\odot$ , and  $i=65^\circ$ . These were chosen as they are consistent with our estimated system parameters (see Section 5.2) and appear to fit reasonably well to the position of the two stars in the maps.

In the H I maps (Figs. 5 and 6) the accretion disk itself can be seen in absorption (particularly well in the H  $\gamma$  and He I  $\lambda 4472$  lines maps). The line emission is clearly separated into the two components: emission from the irradiated side of the secondary and from the disk. The disk emission is not azimuthally symmetric, but appears as a bright elliptical ring. The ring is similar to the signature generated by spiral structure in the disk, as seen in the simulations of, e.g. Steeghs & Stehle (1999). Arguably the emission extends



**Figure 4.** The variation of the H  $\beta$  profile over an orbital cycle. The spectra are phase-binned to  $0.1P_{\text{orb}}$ . The flux scale is relative intensity.

further along the spiral arms in H  $\gamma$  than in H  $\beta$ , particularly the arm which curls around to the upper right of the secondary emission in the maps. The spiral structure of the emission explains the deviation from a pure Gaussian of the line profile, which leads to distortion of the radial velocity curve in Fig. 3.

The He I lines are much weaker than the H lines, yet we still manage to extract some information about the distribution of He I in the accretion disk by creating a Doppler map from He I  $\lambda 4472$ . This line is blended with a weak Mg II  $\lambda 4481$  line, which can be seen in the trailed spectrum as periodic emission at the redward edge of the absorption profile. We were able to include this component as a blend in the Doppler tomogram, but were forced to estimate its strength relative to He I  $\lambda 4472$ . However, we can see in Fig. 7 that He I  $\lambda 4472$  follows the same spiral structure as H  $\gamma$  and H  $\beta$ . It is also just possible to discern a faint emission centred on the secondary, but it is much weaker than in the H I maps. The emission is, however, clearly present in the trailed spectrum. The relative strength of the emission, compared to absorption, is significantly weaker than for the hydrogen lines.

The low S/N ratio of the He I  $\lambda 4922$  line precludes us from constructing a reliable Doppler map, likewise for He II  $\lambda 4686$ . However we have plotted their phase-folded trailed spectra in Figs. 8 and 9. From the trailed spectrum of He I  $\lambda 4922$  we can discern the bright narrow emission that we have attributed to the irradiated secondary. We also see

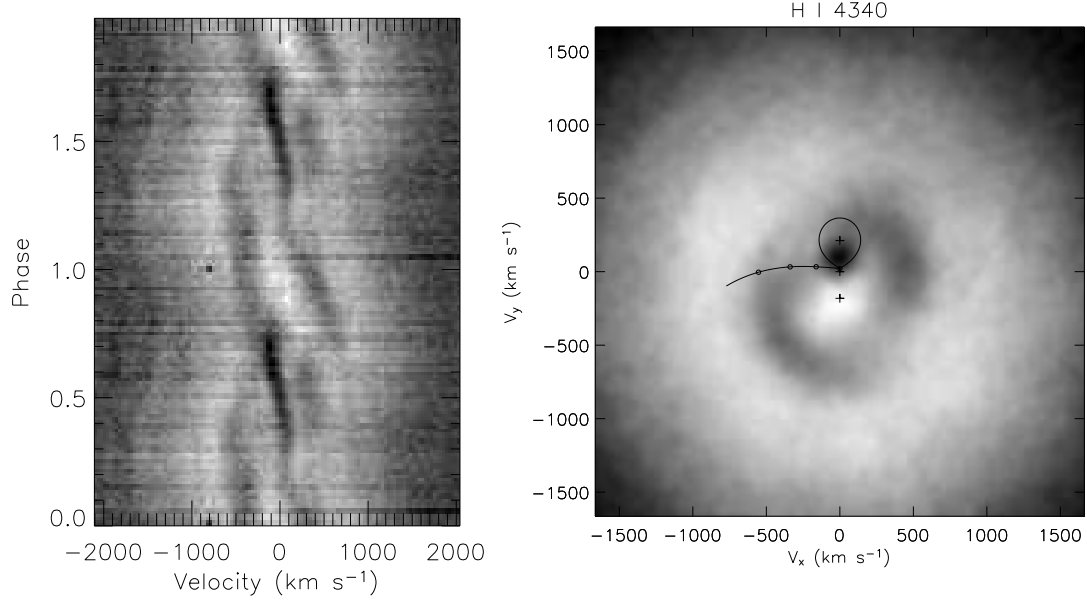


**Figure 5.** Trailed spectrum and Doppler tomogram of the H  $\gamma$  line. Marked on the map are the locations of the primary, secondary and system centres of mass; the Roche lobe of the secondary; and the accretion stream from the secondary. These were calculated for input parameters of  $M_1=0.7M_\odot$ ,  $M_2=0.6M_\odot$ , and  $i = 65^\circ$ . The flux scale is from white to black (i.e. strongest absorption in white, emission in black).

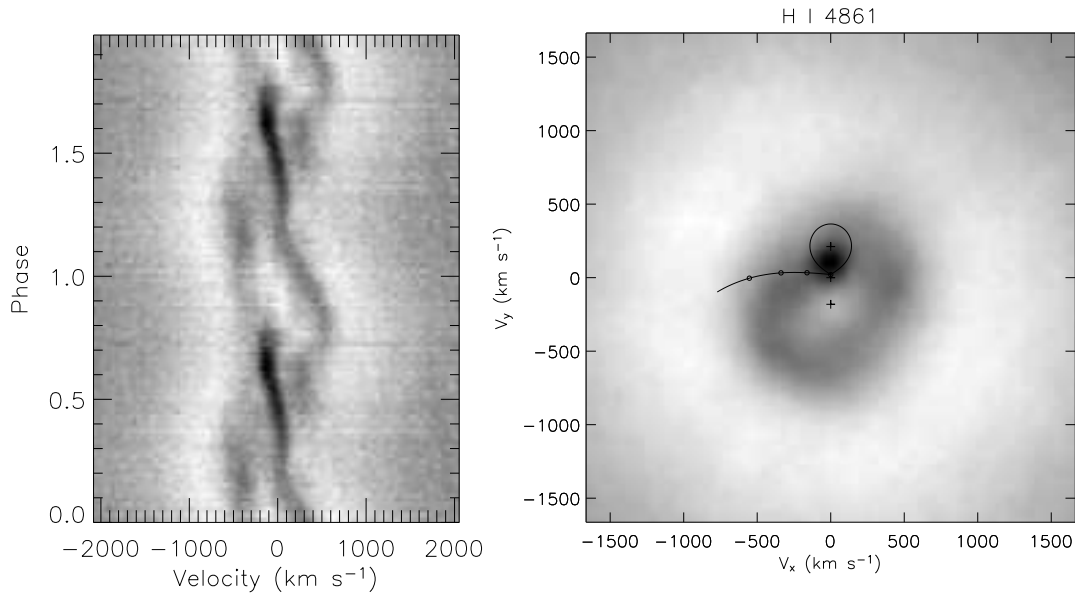


**Figure 6.** Trailed spectrum and Doppler tomogram of the H  $\beta$  line. Markings are as for Fig. 5.

the S-wave structure, which is revealed as spiral arms in the H I maps. Less structure is visible in He II  $\lambda$  4686, although we can just make out a darker structure (corresponding to emission) moving bluewards at phase 0.8 to 1.2, which in the H  $\beta$  and H  $\gamma$  trailed spectra is associated with the spiral seen in the upper-right quadrant of the Doppler maps.

#### 4.2 Irradiation of the secondary star

To measure the strength of the narrow emission requires that it first be isolated from the complex underlying line structure. To do this we first radial-velocity corrected each individual spectrum to remove the WD orbital motion. From

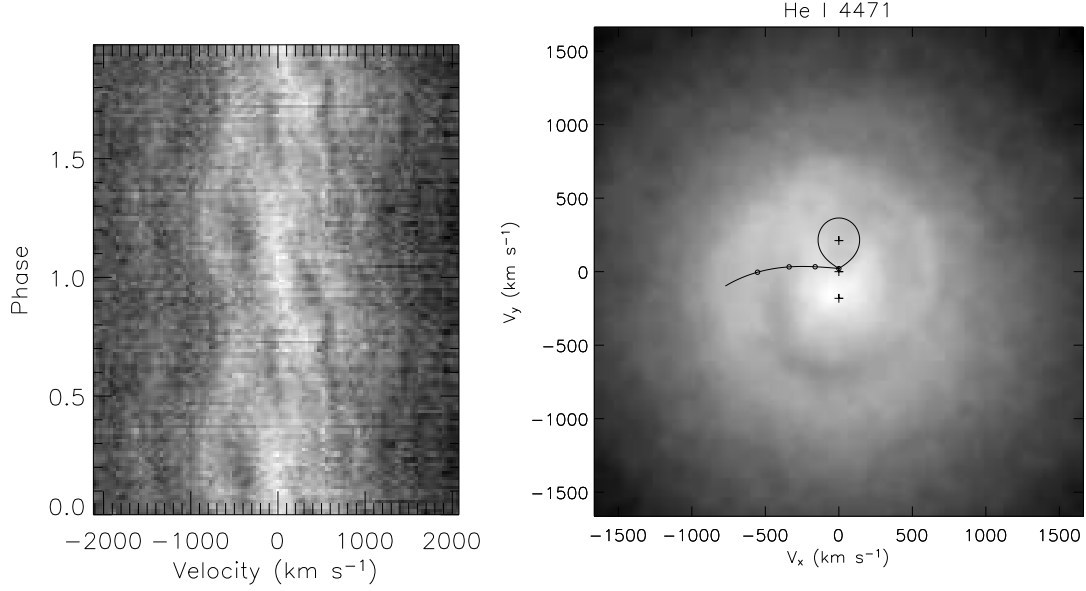


**Figure 7.** Trailed spectrum and Doppler tomogram of the He I  $\lambda$  4471 line. Markings are as for Fig. 5.

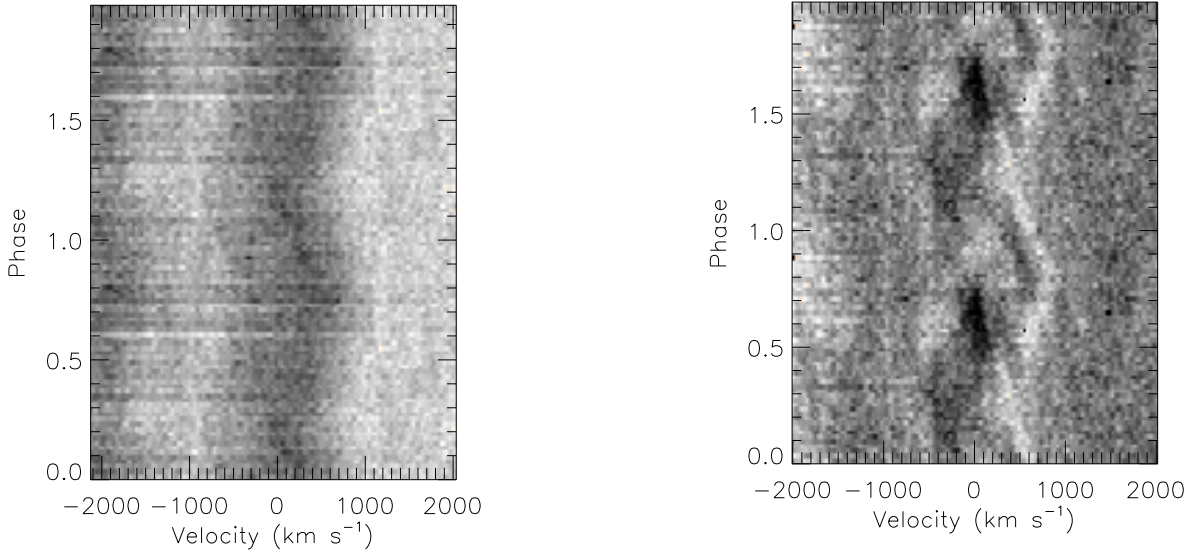


**Figure 8.** Trailed spectrum of the He I  $\lambda$  4686 line.

**Figure 9.** Trailed spectrum of the He I  $\lambda$  4922 line.

the corrected spectra a time-average was created, which was used to normalise each radial-velocity corrected spectrum. Finally, these normalised spectra were phase binned to a resolution of  $0.02P_{\text{orb}}$ . As the underlying broad absorption and double-peaked emission remains fairly constant over the orbital cycle, the only feature that varies significantly in the normalised spectra is the narrow emission, thus we were able to measure the variation in the narrow emission flux (see Fig. 10).

The narrow emission is present in the H  $\beta$  and H  $\gamma$  lines

from phase 0.32 to 0.76, with peak flux centred around phase 0.55. It has a FWHM of around  $150\text{--}200\text{ km s}^{-1}$ . Narrow emission can also be distinguished in He I  $\lambda$  4472 and  $\lambda$  4922, but appears later at phase 0.50 to 0.76, with a peak at phase 0.55. However, the S/N of this narrow component is very low and so hard to distinguish from the other line components. There is no evidence of narrow emission in He II  $\lambda$  4686, nor in the C III–C IV–N III complex.

The radial-velocity curve of the narrow H  $\beta$  emission is antiphased to that of the broad absorption. So the narrow

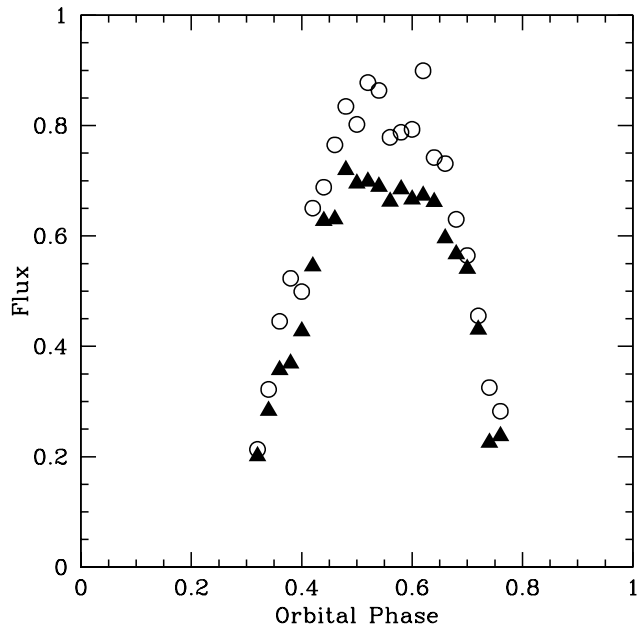


**Figure 10.** Variation in the flux of the narrow emission feature over an orbital cycle, showing H $\beta$  (open circles) and H $\gamma$  (filled triangles). The two line fluxes have a FWHM of  $\sim 0.4$ .

emission most probably emanates from an irradiated region on the the secondary star facing the WD. This would also explain the disappearance of the emission when irradiated side of the secondary rotates away from us (around phase 0). The narrow emission peaks in strength at phase 0.55. We would expect irradiation of the secondary solely by the WD and inner disk to give rise to emission appearing symmetrically around phase 0.5, whereas the peak emission lags the orbital motion by  $0.05P_{\text{orb}}$  (its appearance and disappearance also shows roughly the same phase lag). This suggests either that the irradiating source is offset from the line of centres of the binary system, consistent with a hot-spot formed at the point of impact of the accretion stream on the outer disk, or that the the irradiation due to the WD is impeded by, for example, vertical disc structure.

## 5 DISCUSSION

We have measured the spectroscopic orbital period of V3885 Sgr at  $4.97126 \pm 0.00036$  h. The emission and absorption line profiles and the Doppler maps created from them have revealed:

- the irradiated inner surface of the companion star
- the accretion disc, showing spiral structure, but no sign of any bright spot at the outer edge.

### 5.1 Irradiation of the secondary

The narrow line emission associated with the irradiated companion is seen in the H lines, lasting from  $\phi = 0.32$ – $0.76$  and peaking at  $\phi = 0.55$ . In He I the same narrow emission appears later at  $\phi \simeq 0.5$ . It is not seen in He II  $\lambda 4686$ , nor the nearby N III–C III–C IV blend. The anti-phasing of the

narrow emission component to the disk-formed absorption (Fig. 3) places it on the Doppler maps (Figs 5 to 7) at the inner edge of the companion star, suggesting that this area is being heated by some irradiating source.

To better understand the emission mechanisms at work in V3885 Sgr, we find it helpful to continue our comparison with the other bright nova-like variable, IX Vel (see Hartley et al. 2002). A detailed spectral analysis of IX Vel, covering the same spectral range as in this paper (as well as H $\alpha$ ), is presented by Beuermann & Thomas (1990, hereafter BT90). In IX Vel the same narrow H $\beta$  emission is seen to peak in strength at  $\phi = 0.55$ . However, it is visible over the whole orbital cycle (although BT90 admit that this could be due to confusion between the narrow and broad components). In IX Vel, the variation of line flux with phase has a narrower FWHM of 0.35, compared to 0.4 for V3885 Sgr (Fig. 10).

BT90 model the variation of line flux produced by irradiating the secondary from a bright spot at the outer edge of the disk and from the WD (or boundary layer). They conclude that, to explain the offset in peak flux from phase 0.5 to phase 0.55, some contribution from the bright spot to the irradiating flux is probably required. However, if we were to accept the bright spot as the irradiating source for V3885 Sgr, we would expect it to be a visible component in the Doppler maps (e.g. Harlaftis & Marsh 1996).

In explaining the irradiation of the secondary during an outburst of the dwarf nova IP Peg, Marsh & Horne (1990) discount the bright spot as the ionising source because the secondary is not seen to be irradiated in quiescence, when the bright spot should presumably be relatively brighter. They propose the boundary layer as the irradiating source from which photons in the hydrogen, but not helium Lyman continuum reach the secondary star (in common with V3885 Sgr, IP Peg shows irradiation of the secondary in H $\beta$  and H $\gamma$  but not He II  $\lambda 4686$ ).

We consider that a more plausible alternative to bright-spot irradiation is an irradiating source located close to the WD, either at the inner disk or boundary layer. In this scenario absorption by vertical structure in the accretion disk distorts the radiation field, causing the observed asymmetric irradiation pattern. Likely sources for such structure are the spiral waves themselves, or the overflow of the accretion stream across the surface of the disk. As the resolution of our maps is at present, not sufficient to reveal the distribution of either of these features in the inner disk region, it is impossible to speculate any further.

### 5.2 System parameters

Estimates of the binary parameters of V3885 Sgr have been scarce hitherto. However, it is possible to use our measured  $K$ -velocities to constrain the component masses and system inclination.

In Fig. 11 we see the limits placed on the mass ratio,  $q$ , by our measured values of  $K_1$  (the WD  $K$ -velocity) and  $K'_2$  (the  $K$ -velocity of the irradiated inner surface of the secondary). These allow us to constrain  $K_2$  (the secondary  $K$ -velocity) in several ways: 1) it must be larger than  $K'_2$  (solid line); 2)  $K'_2$  cannot be less than the  $K$ -velocity at the inner Lagrangian point (dashed line); 3)  $K_2 = K_1/q$  for  $K_1 = 166 \text{ km s}^{-1}$  (dot-dashed line).

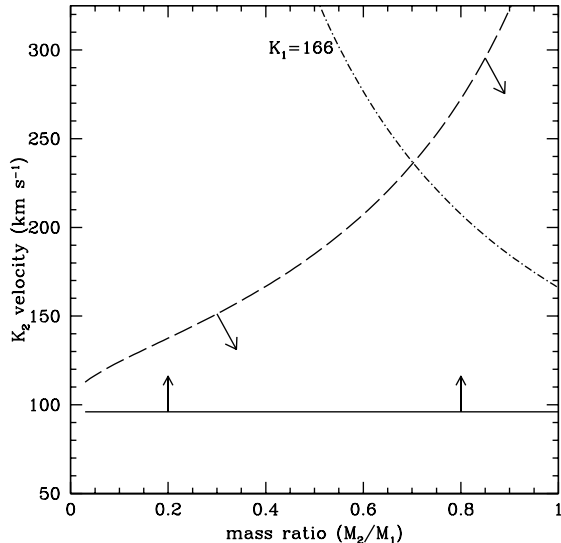


**Figure 11.** Constraints to the value of  $K_2$  as a function of mass ratio (as in Fig. 5 of Steeghs & Casares 2002). The horizontal solid line is the lower limit on  $K_2$ , given our measured  $K'_2$ . The dashed line gives an upper limit on  $K_2$ , given that the velocity of the  $L_1$  point may not exceed  $K'_2$ . The dot-dashed lines indicate  $K_2$  given the relationship  $K_2 = K_1/q$ .

From Fig. 11 we see that a mass ratio  $q \gtrsim 0.7$  is required to reconcile the two  $K$ -velocity measurements. We get an independent estimate of the WD mass with the relation  $M_2 \simeq 0.11 P_{\text{orb}} (\text{h})$  (King 1988). For V3885 Sgr,  $P_{\text{orb}} \simeq 5 \text{ h}$ , which translates to a secondary mass of  $\simeq 0.55 M_\odot$ . For  $q \gtrsim 0.7$  this requires  $M_1 \lesssim 0.8 M_\odot$ . It is also possible to calculate  $K_2$  as a function of  $q$  for a given system inclination and WD mass. For the constraints on  $K_2$  and  $q$  in Fig. 11 and our upper estimate of  $M_1 = 0.8 M_\odot$ , this would suggest  $i > 85^\circ$ : implausible for a non-eclipsing system. At a lower limit of  $M_1 = 0.55 M_\odot$ , i.e.  $q = 1$ , the inclination would have to be about  $65^\circ$  for the system to lie on the dot-dashed line in Fig. 11. While these masses and inclinations are pure estimates, it would seem that an inclination of  $> 65^\circ$  and primary mass of  $0.55 < M_1 < 0.8 M_\odot$  are sensible limits for V3885 Sgr.

We can briefly compare the system parameters of V3885 Sgr and IX Vel. BT90 derive an inclination  $i = 60 \pm 5^\circ$  for IX Vel. The difference in the phase coverage of the narrow emission in the two systems could point to a higher inclination for V3885 Sgr, which would be supported by its higher  $K_1$ -velocity ( $166 \text{ km s}^{-1}$  vs.  $138 \text{ km s}^{-1}$ ). However, it is equally plausible that the irradiated region of the secondary is smaller in V3885 Sgr than in IX Vel, which would give the same effect. Hartley et al. (2002) argue that, given their similar UV spectra and their relative distances, the systems are of similar inclinations, but that IX Vel could be the more luminous by a factor of up to two. Assuming that the luminosity is due to accretion, then the mass accretion rate in IX Vel could be one to two times higher than in V3885 Sgr. This would result in a brighter or more extended irradiated region on the secondary. If the irradiated region were smaller in V3885 Sgr this could explain why V3885 Sgr has a larger ratio of  $K_1/K'_2 = 166/96$  than IX Vel ( $K_1/K'_2 = 138/108$ ,

BT90); the smaller the irradiated region, the larger the difference between  $K_2$  and  $K'_2$ .

There is scant evidence in the literature to favour any particular inclination for V3885 Sgr and little agreement between studies: Cowley et al. (1977) saw no evidence for eclipsing, whereas Haug & Drechsel (1985) thought they did. Acquiring good continuum light curves of V3885 Sgr is now a priority, both for the sake of being better able to compare V3885 Sgr to similar systems and because a reliable measurement of the inclination will allow us to better understand the how disk geometry affects the irradiation of the secondary star.

### 5.3 Spiral structure in accretion disks

In V3885 Sgr we have seen the first conclusive evidence for persistent spiral structure in the disk of a novalike variable. Interestingly, the spiral waves are apparent only in H I and He I, but not in the higher-ionisation He II and N III–C III–C IV lines. This is at odds with observations of dwarf novae in which the spirals are typically also detected in He II  $\lambda 4686$ : IP Peg (Harlaftis et al. 1999), WZ Sge (Kuulkers et al. 2002), SS Cyg (Steeghs et al. 1996) and U Gem (Groot 2001). In our data the He II and N III–C III–C IV lines appear to be wind-formed, so any disk structure in these features has been submerged beneath the wind emission.

Both theory and simulation tell us that a steady state, viscous accretion disk will not be axially symmetric about the accreting star. For the disk to reach a steady state it must be large enough for tidal removal of angular momentum to occur. In other words, the disk must be large enough to be perturbed by the gravitational field of the secondary star. We know (from, e.g. Paczynski 1977) that the magnetic field of the secondary will impose an elliptical perturbation on the disk. The orientation of this perturbation is fixed in the binary frame, making this the best frame in which to imagine the behaviour of the gas. As gas passes around the primary it experiences two periods of compression and two of rarefaction. The compression can be dramatic enough as to cause the flow in the outermost regions of the disk to shock. The vertical extent of the outer disk will also vary quite dramatically as the gas alternately compresses and expands (again this variation will be stationary in the binary frame).

That elliptical variations should occur in the outer regions of CV disks in the high state is uncontroversial. There is less agreement as to the degree to which these perturbations propagate into the inner disk as spiral shocks, perhaps carrying significant net (negative) angular momentum with them. Until now, observable elliptical disk structure has been primarily associated with dwarf novae in outburst. In these systems however, the large variations in disk structure (radius, thermodynamic properties, ‘viscosity’ etc.) that occur over the course of an outburst make it difficult to isolate the importance of any spiral structure. In a novalike variable, however, the disk is both large and stable, so these should be the best systems in which to analyse spiral shocks.

The lack of identifications of elliptical disk variations in novalike variables has been disappointing. Although Doppler maps for at least sixteen novalike variables have been published, elliptical disk structure has been sighted (tentatively) only in the eclipsing system V347 Pup (Still et al. 1998). It

has been argued that in novalikes any signatures from the disk would be obscured by an outflow. However, our data show that while wind emission appears to be obscuring spiral structure (if it is present) in the He II and N III–C III–C IV lines, the H I and He I lines appear untainted by the outflow. Therefore, the absence of disk signatures from novalike systems, while they are detected in dwarf novae remains puzzling. A lack of good quality spectra could be responsible, and a re-examination of particularly the bright novalike variables now seems justified.

V3885 Sgr is so bright that it holds the prospect of being the one of the best candidates for studying the importance of non-axisymmetric accretion disk structure, and higher resolution observations are both feasible and called for. Our time and wavelength resolution are not quite sufficient for us to either measure the pitch angle of the spiral structure (how tightly wrapped the spirals are), or estimate the disk radius to which it penetrates. The former measurement would give us the Mach number of the flow in the outer disk whilst the latter would provide a measure of the local dissipation.

An important consideration in interpreting these results lies in relating the emission regions to the shocks that underly them. In particular, it is not clear how the energy released by the shocks (presumably near the disc midplane where densities are highest) finds its way to the upper atmosphere of the disc where emission lines are excited. This remark applies quite generally to all observations of disk structures. Numerical simulations offer little insight, as they invariably incorporate a very simple (adiabatic, polytropic or isothermal) equation of state for the gas with little or no accounting made of radiative transport (see, e.g. Boffin 2001).

It may not even be necessary to resort to spiral shocks. Recent observations of spiral patterns in the disks of quiescent dwarf novae (see Morales-Rueda 2004, and references therein) imply that energy dissipated by spiral shocks may not be responsible for the observed pattern. Instead we may simply be seeing the tidally thickened regions of the outer disk, illuminated by light from the inner disk or boundary layer. From the point of view of V3885 Sgr this is an attractive model, as the spirals appear in tandem with irradiation of the secondary star. The same source of photons could be responsible for both emission patterns, particularly as we require the disk to be absorbing some of the boundary layer radiation to account for the asymmetry of the secondary irradiation pattern.

Clearly, if the spirals which we have seen in the disk of V3885 Sgr are caused by the same mechanism as the more widely-observed spiral structure in dwarf novae, then any explanation of this phenomenon must be applicable to both steady-state and thermally unstable disks. Further observations of novalike systems (the most obvious candidate being IX Vel) are called for in order to better understand the three-dimensional structure of disks in binaries.

## REFERENCES

- Beuermann K., Thomas H.-C., 1990, AA, 230, 326  
 Boffin, H.M.J., 2001, LNP Vol. 573: Astrotomography, Indirect Imaging Methods in Observational Astronomy, 69  
 Cowley A.P., Crampton D., Hesser J.E., 1977, ApJ, 214, 471  
 Drew J.E., Hartley L.E., Long K.S., & van der Walt, J. 2003, MNRAS, 338, 401  
 Groot P.J. 2001, ApJL, 551, L89  
 Harlaftis E.T. & Marsh T.R. 1996, A&A, 308, 97  
 Harlaftis E.T., Steeghs D., Horne K., Martín E., Magazzú A., 1999, MNRAS, 306, 348  
 Hartley L.E., Drew J.E., Long K.S., Knigge C., & Proga D. 2002, MNRAS, 332, 127  
 Haug K., Drechsel H., 1985, AA, 151, 157  
 King A. R., 1988, QJRAS, 29, 1  
 Kuulkers E., Knigge C., Steeghs D., Wheatley P.J., & Long K.S. 2002, ASP Conf. Ser. 261: The Physics of Cataclysmic Variables and Related Objects, 443  
 Marsh T.R. & Horne K., 1988, MNRAS, 235, 269  
 Marsh T.R. & Horne K. 1990, ApJ, 349, 593  
 Metz K., 1989, IBVS, 3385, 1  
 Morales-Rueda L. 2004, AN, 325, 193  
 Paczynski, B., 1977, ApJ, 216, 822  
 Steeghs, D., & Stehle, R. 1999, MNRAS, 307, 99  
 Steeghs D. & Casares J., 2002, ApJ, 568, 273  
 Steeghs D., Horne K., Marsh T.R., & Donati J.F. 1996, MNRAS, 281, 626  
 Still M.D., Buckley D.A.H., & Garlick M.A 1998, MNRAS, 299, 545  
 Woods J.A., Verbunt F., Collier Cameron A., Drew J.E., & Piers A. 1992, MNRAS, 255, 237